UCRL-JC-106803
PREPRINT

RADIATION FROM WIGGLERS IN THE LOW ENERGY RING OF AN ASYMMETRIC B FACTORY

William A. Barletta

This paper was prepared for submittal
to the Proceedings of the Workshop on
Rare B&K Decays and Flavor Factories
Santa Monica, CA, February 12-14, 1991

March 21, 1991

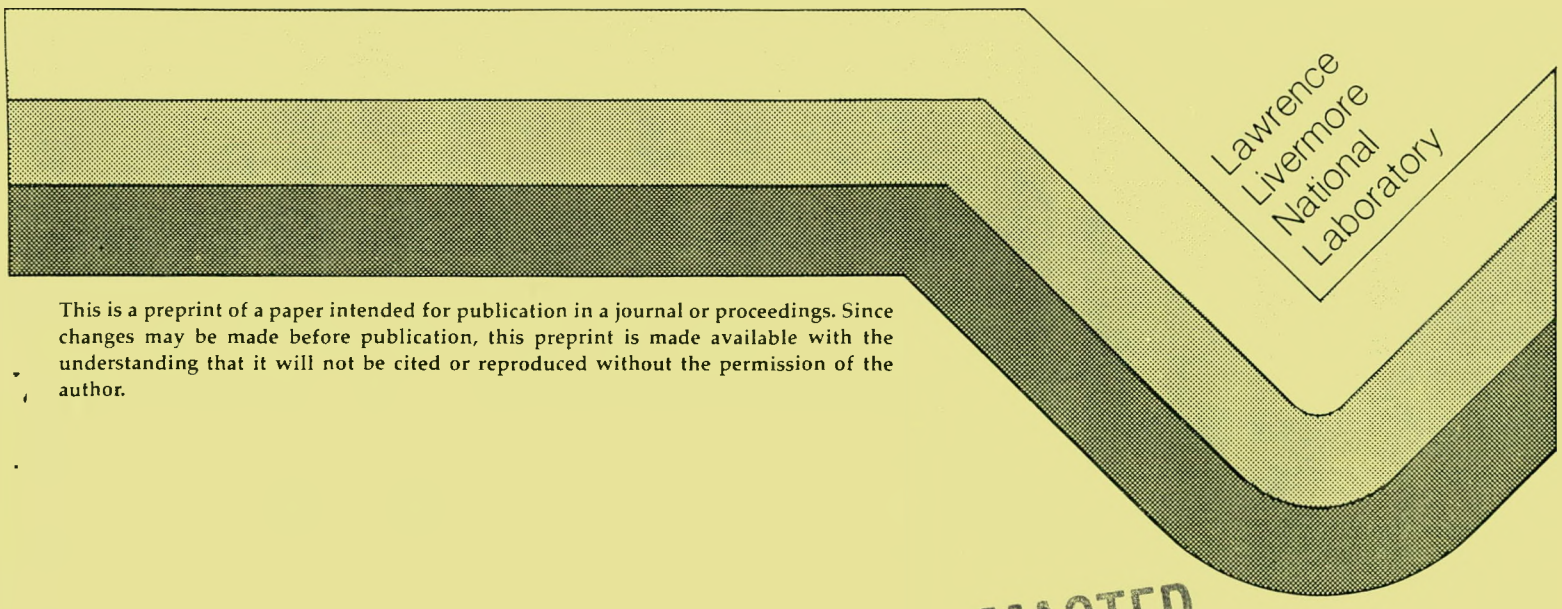

UCRL-JC--106803

DE91 010474

RADIATION FROM WIGGLERS IN THE LOW ENERGY RING OF AN ASYMMETRIC B FACTORY

William A. Barletta

Lawrence Livermore National Laboratory
and
Department of Physics, University of California Los Angeles

ABSTRACT

We compute the angular distribution of radiation in the near field of a long damping wiggler that is required to determine the equilibrium emittance and the damping decrement in the low energy ring of a high luminosity B factory. From the power distribution we can estimate the size of the vacuum chamber, the photon channel, and the photon dump that can tolerate the enormous average power of x-rays generated in the wiggler.

INTRODUCTION

Earlier studies of asymmetric B factories ["Feasibility Study of an Asymmetric B-Factory based in the PEP Tunnel", LBL PUB-5244, Oct. 1989 and "Investigation of an Asymmetric B-Factory based in the PEP Tunnel", LBL PUB-5263, March 1990] have argued for the potential advantages of having equal damping decrements in the high- and low-energy rings in order to minimize the effects of the energy asymmetry on the beam-beam interaction. Should continuing studies of beam stability confirm the desirability of operating the collider with equal damping decrements, the energy loss per turn, U_0, in the low energy ring can be increased through the use of wigglers. The damping decrement for a storage ring of energy, E, can be written as

$$\Lambda = \frac{T_0}{\tau_x} = \frac{U_0}{2E}, \tag{1}$$

where T_0 is the revolution period and τ_x is the damping time. Equal damping decrements in the high-and low-energy rings imply that the energy loss per turn due to synchrotron radiation must scale in proportion to the beam energy in the ring. In the 9 GeV, high-energy electron ring of APIARY, the energy loss is dominated by bending magnet radiation in the arcs with a magnetic radius (ρ = 165 m). The energy loss is given by

$$U_0 = 0.0885 \frac{E^4}{\rho}, \tag{2}$$

which gives U_0 = 3.52 MeV/turn; losses in other magnets bring the total loss to 3.6 MeV/turn in the high energy ring. For equal damping decrements the energy loss in the low-energy, positron ring should be

$$U_{0,+} = U_{0,-}\frac{E_+}{E_-} = 3.6\left(\frac{3.1}{9.0}\right) = 1.24 \text{ MeV/turn} \quad (3)$$

In the low-energy ring lattice of APIARY, the bend radius in the arcs is ρ = 30.6 m which implies that U_0 = 0.27 MeV/turn, only about one-fifth of the requisite loss. (Matching damping decrements from the bending magnet radiation alone would require a bend radius of 6.75 m, which would be impractical with respect to the thermal power density on the walls of the vacuum chamber.) To the loss in the arcs, we must add the radiation loss from other magnets such as the vertical bends that separate the two beams beyond the interaction region and bending magnets that may be used to steer the beam into damping wigglers. By scaling Eq. (2) for the low energy beam, we find that the vertical bends contribute 0.014 MeV/turn.

To equalize the damping decrements in the two rings we must increase the energy loss of the low energy beam by an additional 0.96 MeV/turn through the use of arrays of wiggler magnets located in straight sections of the low energy ring. The wigglers have a second critical function in the low energy ring, namely, increasing the emittance of the beam to yield the tune shift limited luminosity. Consequently, the characteristics of the wiggler must be chosen to balance the requirements of tuning the emittance in the low energy ring, of managing the energy loss, and of confining the multi-MW synchrotron radiation fan in a practically sized vacuum chamber. By locating the wiggler at a shallow horizontal tilt with respect to the principal axis of the straight section, the rms dispersion (and therefore the emittance growth) in the wiggler can be controlled external to the wiggler by dipoles on either side of the wiggler. This additional degree of freedom extends the range of allowable wiggler characteristics. Removing the wiggler from the principal axis of the beamline also allows us to project the intense radiation fan into a far away dump. The bend magnets used to divert the beam into the wiggler, themselves lead to an additional loss of 0.03 Mev/turn.

We have conformed to the following constraints in designing the damping wigglers:

- Wigglers occupying no more than 2 straight sections,
- No more than 2 kW/cm^2 power deposited on the walls of the vacuum chamber or on the beam dump,
- Total energy loss in wigglers of 0.93 MeV/turn,
- Maximum practical wiggler field of 1.8 T.

Within these constraints we have considered two configurations:

1) a bend-drift configuration calculated with dipoles of constant magnitude field and
2) a standard wiggler with a dipole field varying sinusoidally along the beam path.

In the bend drift configuration, two identical wiggler arrays are each composed of four segments of alternating dipoles that cause the beam to wiggle in the horizontal plane. These dipoles are arranged in the horizontal chicane as displayed schematically in Fig. 1. The lengths of all of the segments of the wiggler are equal; $L_1 = L_2 = L_3 = L_4 = 6$ m. The total length of wiggler segments, L_w, is thus 24 m. The dipoles each have a length of 20 cm, a field, B_w, of 1.63 T. The drift space between dipoles is 13.3 cm. This arrangement yields a 60% fill factor, F_{fill}, with an effective wiggler period, λ_w, of 66.6 cm. A space, d, of 5.0 m between the two wiggler sections L_2 and L_3 allows for a quadrupole triplet that provides focusing in the wiggle (horizontal) plane.

A detailed diagram of the lattice functions of the wiggler as matched into the low energy ring corresponding to the case of equal damping times is displayed in Fig. 2 [Al Garren, Private communication, 1991]. The optics of the wiggler straight section are symmetric about the center of the wiggler. Seven independent quadrupoles produce a beam waist at the center of the wiggler and bring the dispersion to zero there. This arrangement causes the dispersion and its slope to be zero at either end of the straight section.

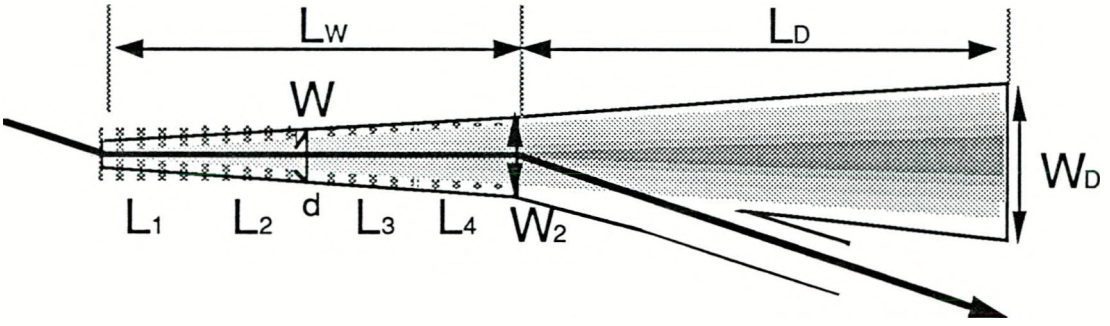

Figure 1. Schematic representation of bend-drift wiggler and the vacuum chamber in the region of the damping wigglers.

PROPERTIES OF WIGGLER RADIATION

Given the wiggler field, B_w, and the period, λ_w, one can describe the properties of the wiggler radiation from either configuration in terms of an equivalent sinusoidal wiggler. For a wiggler field that varies sinusoidally along the beam path, the integrated energy loss per wiggler period is given by

$$U_{0,w}\,(\text{MeV/turn/period}) = 6.33 \times 10^{-6}\, E^2\, B_w^2\, \lambda_w\,, \tag{4}$$

whereas for a bend-drift configuration

$$U_{0,w}\,(\text{MeV/turn/period}) = 1.267 \times 10^{-5}\, E^2\, B_w^2\, \lambda_w\, F_{fill} \tag{5}$$

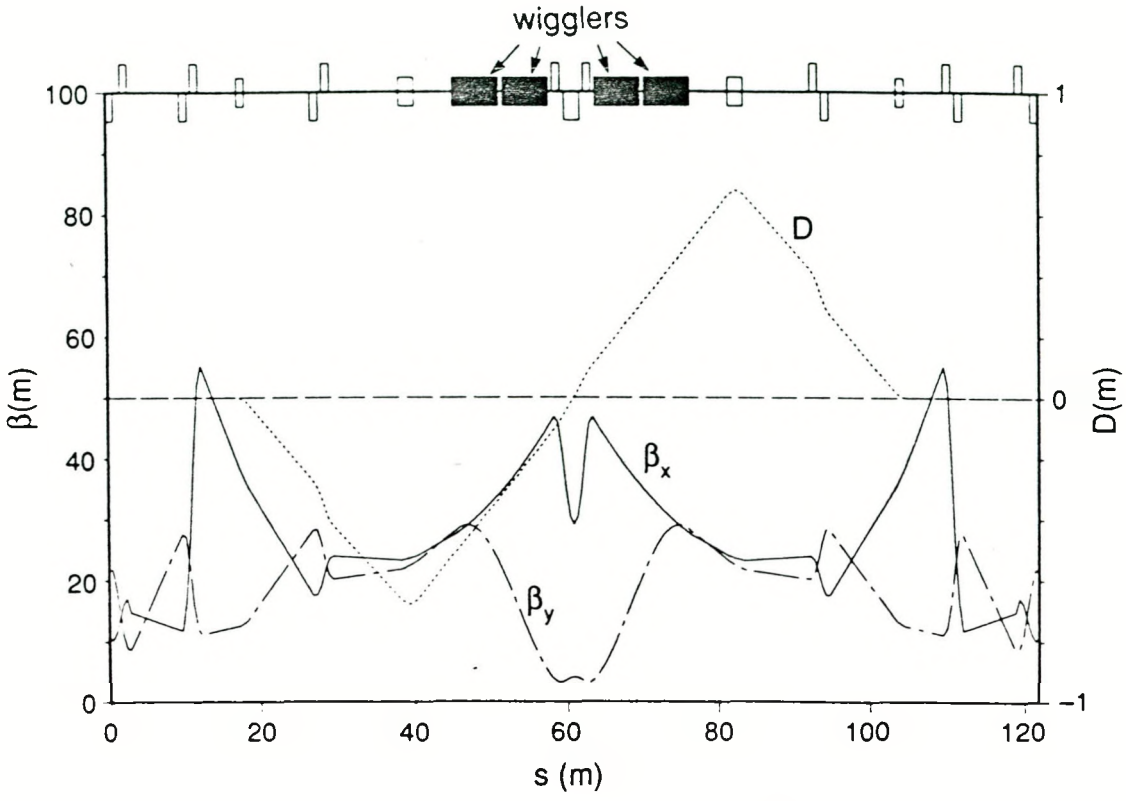

Figure 2. Layout and optics functions for the wiggler straight sections of the low energy ring. In conjunction with the dispersion function D, and its derivative, the wigglers increase the emittance of the low-energy beam. In addition, the wigglers can decrease the damping time of the low-energy beam so that it is equal to that of the high-energy beam.

where the beam energy, E is in GeV, B_w is the peak wiggler field in T, and λ_W is the wiggler period in cm. Consistent with the design constraints described in Section I, the 48 meters of wiggler with a field, B_w, of 1.63 T will provide the additional 0.93 MeV/turn needed to equalize the damping decrements in the two rings.

At the maximum limiting current of 3 A, each wiggler will produce about ≈1.4 MW of synchrotron radiation power. The majority of this power must be dumped external to the vacuum chamber of the low energy ring in specially designed photon beam dumps. Some of the power will, however, be deposited on the side walls of the vacuum chamber in the vicinity of the wiggler. To compute the power density at the dump and on the walls, we must estimate the angular distribution of the radiation. The geometry of the calculation is illustrated in Fig. 3.

A precise description of radiation from non-sinusoidally varying wigglers in the near field is not given in the literature. We can, however, modify the far field descriptions for standard wigglers given by Kim ["Angular distribution of undulator power, Nuc. Inst. and Meth., A246 (1986)] to describe segments of the wiggler to

evaluate the vacuum system characteristics. Denoting the horizontal angle by θ and the vertical angle by ψ, we can write the power density in W/mr^2 as

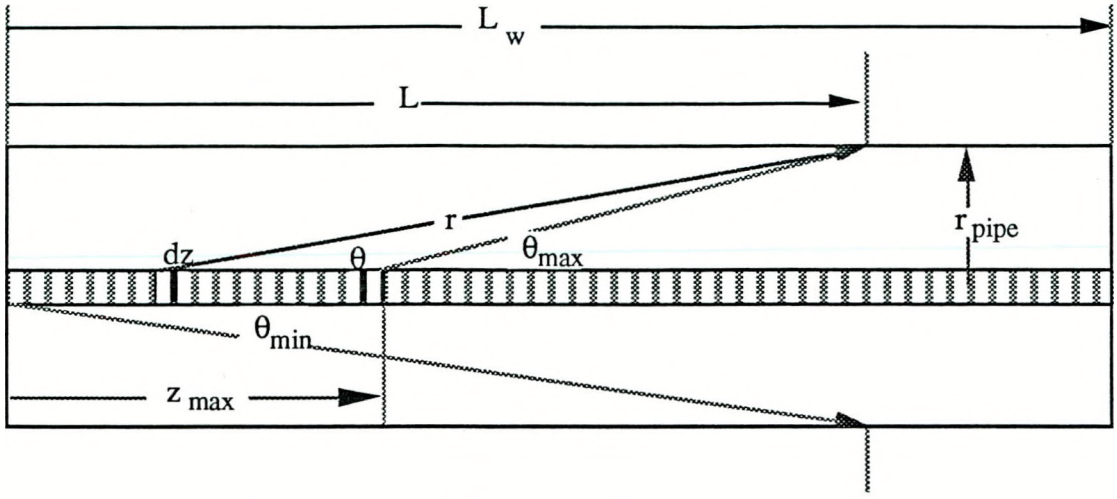

Figure 3. Geometry of radiation deposition on the vacuum chamber.

$$\frac{dP}{d\Omega}(\theta,\psi) = \frac{21\,\gamma^2}{16\,\pi\,K}\,U_{0,w}\,I(A)\,N_W\,G(K)\,f_K(\gamma\theta,\gamma\psi)\,, \qquad (6)$$

where N_w is the number of periods, I is the beam current, and K is the wiggler parameter. For a standard wiggler with B varying sinusoidally along the beam path,

$$K = 0.934\;B_w(T)\,\lambda_w(cm)\,. \qquad (7)$$

The normalization factor G(K) in Equation (6) is

$$G(K) = K\frac{\left(K^6 + \frac{24}{7}K^4 + \frac{16}{7}\right)}{\left(1+K^2\right)^{7/2}}. \qquad (8)$$

For $K >> 1$, $G(K) \approx 1$; moreover, the angular distribution is sharply cutoff in the wiggler's bend plane. In the limit of $K \rightarrow \infty$, the angular distribution function, $f(\gamma\theta,\gamma\psi)$, normalized to $f_K(0,0) = 1$ is given by

$$f_K(\gamma\theta,\gamma\psi) = \sqrt{1-\left(\gamma\theta/K\right)^2}\;\left\{\frac{1}{\left(1+(\gamma\psi)^2\right)^{5/2}} + \frac{5\,(\gamma\psi)^2}{7\left(1+(\gamma\psi)^2\right)^{7/2}}\right\}. \qquad (9)$$

From Eq. (9) one sees that the radiation is spread over an horizontal angle, $2\theta_w$, where

$$2\,\theta_w = \frac{2\,K}{\gamma}\,. \tag{10}$$

In the non-bend plane (vertical) plane, the synchrotron radiation is spread over an rms angle

$$\psi_w = \left(\frac{\varepsilon_y}{\beta_y} + \frac{0.79}{\gamma^2}\right)^{1/2}\,. \tag{11}$$

As one sees in Fig. 4, for $K > 1$ approximately 20 % of the radiation is emitted at angles greater than $|\psi_w|$; approximately 15 % of the radiation is emitted between $1.0\,\psi_w < |\psi| < 1.5\,\psi_w$. The full-width-half-maximum vertical angle of the radiation is $1.3/\gamma$.

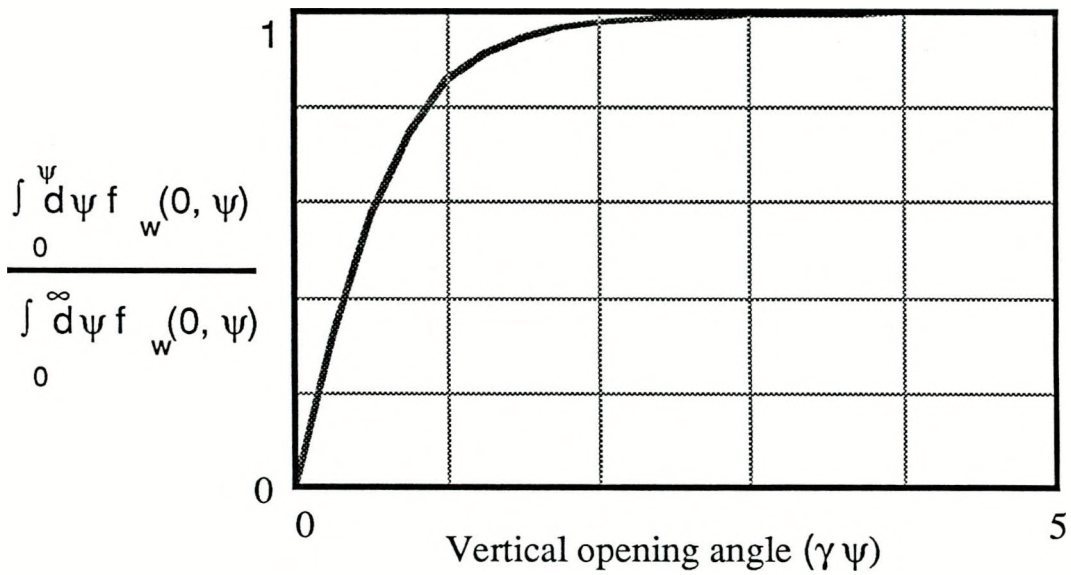

Figure 4. Synchrotron radiation power integrated over vertical opening angle.

For the bend-drift configuration we can approximate the radiation properties of the wiggler by replacing K in Eq. (6) through (9) with an effective wiggler parameter, K_{eff}, such that

$$\theta_{bend} = \frac{2\,K_{eff}}{\gamma}\,. \tag{12}$$

In Eq. (12) θ_{bend} is the full angle of the bend in one of the bending dipoles of length, L_{dipole}, that constitute the wiggler;

$$\theta_{bend} = \frac{L_{dipole}\,B_w}{(B\rho)}\,. \tag{13}$$

In a more suggestive form,

$$K_{eff} = 1.47\ B_w\,(T)\ \lambda_w\,(cm)\ F_{fill}\ . \tag{14}$$

In designing a vacuum enclosure for the wiggler, one must assure that the power density is less than some specified value ($\approx 1 - 2$ kW/cm^2). We begin by considering the the walls of the vacuum chamber to be parallel to the axis of the wiggler. Referring to Fig. 3, one can compute the density of power deposited at a point L along the wall of the wiggler chamber. In the bend plane the power density from a segment dz is

$$\frac{dP\,(\theta,0)}{dL\ dy}\ \frac{dz}{\lambda_w} = \frac{1}{\lambda_w}\ \frac{dP(\theta,0)}{d\theta\, d\psi}\ \frac{\sin\theta}{r^2}\ dz\ , \tag{15}$$

where y is the normal to the bend plane. Integrating Eq. (15), one has ,

$$\frac{dP\,(L,0)}{dL\ dy} = \int_0^{z_{max}} \frac{P_o \sin\theta}{r^2} \sqrt{1 - \frac{\gamma^2}{K^2}\theta^2}\ dz\ , \tag{16}$$

in which

$$z_{max} = L - \frac{r_{pipe}}{\theta_{max}} \tag{17a}$$

and

$$P_o = \frac{21\,\gamma^2}{16\,\pi\,K}\ \frac{U_o I}{\lambda_w}\ G(K)\ . \tag{17b}$$

For $\theta_{bend} << 1$,

$$\theta = \frac{r_{pipe}}{L - z}\ . \tag{18}$$

Hence, one can rewrite Eq. (16) as

$$\frac{dP\,(L,0)}{dL\,dy} = \int_{\theta_{min}}^{\theta_{max}} \frac{P_o\,\theta}{r_{pipe}} \sqrt{1 - \frac{\gamma^2}{K^2}\theta^2}\ d\theta\ , \tag{19}$$

where

$$\theta_{max} = \theta_w = \frac{1}{2}\,\theta_{bend} \tag{20a}$$

and

$$\theta_{min} = \frac{r_{pipe}}{L} . \qquad (20b)$$

Evaluating Eq. (19) leads to an expression for the power density, namely,

$$\frac{dP(L,0)}{dL\,dy} = \frac{7}{16\,\pi}\,\frac{\gamma^3}{K^2}\,\frac{U_{o,w}\,I}{\lambda_w\,r_{pipe}}\,G(K)\,\sqrt{\left(\frac{K^2}{\gamma^2} - \frac{r_{pipe}^2}{L^2}\right)^3} \quad . \qquad (21)$$

In Eq. (16), (19), and (21) K represents either K or K_{eff} depending on whether the wiggler field is a standard or a bend-drift configuration; likewise, $U_{o,w}$ should be evaluated using either Eq. (4) or (5) respectively.

To estimate the distributed dynamic gas load due to the radiation incident on the walls one must know the linear power density. As an initial estimate one can multiply Eq. (21) by the mean height, $\langle H_y \rangle$, of the radiation fan from $-\psi_w$ to ψ_w to obtain the linear power density. As the height over the rms angle $\pm\psi_w$ contains only 80% of the energy, the actual linear density on each of the side walls is

$$\frac{dP(L)}{dL} = 1.25\,\frac{dP(L,0)}{dL\,dy}\,\langle H_y \rangle . \qquad (22)$$

The mean height of the radiation fan at the position L is

$$\langle H_y \rangle = -\psi_w\,\frac{(L - z_{max})^2 - L^2}{z_{max}} \quad . \qquad (23)$$

A more accurate description of the linear power density is obtained by integrating the angular distribution over ψ; i.e.,

$$\frac{dP(\theta)}{dL}\,\frac{dz}{\lambda_w} = \int_{-\pi/2}^{\pi/2} d\psi\,\frac{dz}{\lambda_w}\,\frac{dP(\theta,\psi)}{d\theta\,d\psi}\,\frac{\sin\theta}{r} = \frac{1.524\,dz}{\gamma\lambda_w}\,\frac{dP(\theta,0)}{d\theta}\,\frac{\sin\theta}{r} \qquad (24)$$

$$\frac{dP(L)}{dL} = \int_{\theta_{min}}^{\theta_{max}} \frac{1.524\,P_o}{\gamma}\,\sqrt{1 - \frac{\gamma^2}{K^2}\,\theta^2}\;d\theta \qquad (25)$$

$$= \frac{0.762\,P_o}{K}\left\{\frac{K^2}{\gamma^2}\left[\frac{\pi}{2} - \sin^{-1}\left(\frac{r_{pipe}\,\gamma}{L\,K}\right)\right] - \frac{r_{pipe}}{L}\,\sqrt{\frac{K^2}{\gamma^2} - \frac{r_{pipe}^2}{L^2}}\right\} .$$

From Eq. (25) one sees that once the characteristics of the wiggler are chosen, the designer of the vacuum system has only one parameter, r_{pipe}, with which to control the power load on (and consequently the photo-desorption from) the side walls. An additional degree of freedom is obtained by tapering the chamber as illustrated in Fig. 1. To evaluate the power load on the walls of a tapered chamber, we can modify the preceding analysis for a chamber with walls parallel to the wiggler axis. Assume that the walls are tapered by an angle $\theta_t << 1$ such that $\theta_t < \theta_{min}$ and that $\theta_t + \theta_{max} << 1$; then the chamber width becomes a function of L,

$$r_{pipe}(L) = r_o + \theta_t L \, . \tag{26}$$

Then, Eq. (19) becomes

$$\frac{dP(L,0)}{dL\,dy} = \int_{\theta_{min}}^{\theta_{max}} \frac{P_o}{r_{pipe}} (\theta - \theta_t) \sqrt{1 - \frac{\gamma^2}{K^2}\theta^2} \, d\theta \tag{27}$$

which is readily integrated to yield

$$\frac{dP(L,0)}{dL\,dy} = \frac{21}{16\pi} \frac{\gamma^3}{K^2} \frac{U_{o,w} I}{\lambda_w r_{pipe}} G(K) \times \tag{28}$$

$$\left\{ \frac{1}{3} \sqrt{\left(\frac{K^2}{\gamma^2} - \frac{r_{pipe}^2}{L^2} \right)^3} - \frac{\theta_t K^2}{2\gamma^2} \left[\frac{\pi}{2} - \sin^{-1}\left(\frac{r_{pipe} K}{L \gamma} \right) \right] + \frac{\theta_t r_{pipe}}{2L} \sqrt{\frac{K^2}{\gamma^2} - \frac{r_{pipe}^2}{L^2}} \right\}$$

In Eq. (28) the dependence of r_{pipe} on L is implicit. For $\theta_t > r_{pipe}/L$, Eq.(28) should be modified by replacing r_{pipe}/L by θ_t in the expression in braces; for $\theta_t > \theta_{max}$ the power density is zero.

A similar analysis for a tapered chamber yields the linear power density on each side wall given by

$$\frac{dP(L)}{dL} = \int_{\theta_{min}}^{\theta_{max}} \frac{1.524\, P_o}{\gamma} \left(1 - \frac{\theta_t}{\theta} \right) \sqrt{1 - \frac{\gamma^2}{K^2}\theta^2} \, d\theta \, , \tag{29}$$

which becomes

$$\frac{dP(L)}{dL} = \frac{0.762\ P_o}{K}\left\{\frac{K^2}{\gamma^2}\left[\frac{\pi}{2} - \sin^{-1}\left(\frac{r_{pipe}\,\gamma}{L\,K}\right)\right] - \frac{r_{pipe}}{L}\sqrt{\frac{K^2}{\gamma^2} - \frac{r_{pipe}^2}{L^2}}\right\} \tag{30}$$

$$- \theta_t P_o \{Corr\} .$$

The correction term for the taper is

$$Corr = \frac{1.524}{K}\left[\frac{K}{\gamma}\log\left(\frac{K/\gamma + \sqrt{K^2/\gamma^2 - r_{pipe}^2/L^2}}{r_{pipe}/L}\right) - \sqrt{\frac{K^2}{\gamma^2} - \frac{r_{pipe}^2}{L^2}}\right]. \tag{31}$$

For $\theta_t > r_{pipe} / L$, the correction term becomes

$$Corr\left(\theta_t > \frac{r_{pipe}}{L}\right) = \frac{1.524}{K}\left[\frac{K}{\gamma}\log\left(\frac{K/\gamma + \sqrt{K^2/\gamma^2 - \theta_t^2}}{\theta_t}\right) - \sqrt{\frac{K^2}{\gamma^2} - \theta_t^2}\right]. \tag{32}$$

For $\theta_t > \theta_w$, power density on the walls is zero.

MANAGING THE UNMANAGEABLE

With these analytical tools we can return to the design of the vacuum channel for the damping wigglers. At the maximum design current of 3 A in APIARY, each wiggler generates 58.2 kW/m. For any sensible choice of beam emittance and β_y in the wiggler, the vertical spread of the radiation is dominated by the $1/\gamma$ term in Eq. (11). Moreover, the most conservative design strategy is to assume that the radiation comes from a beam of zero emittance. In that case the rms angle, ψ_w, is ± 0.13 mrad in the low energy ring. In the horizontal plane the opening half-angle of the radiation is 15.8 mrad; therefore, if the vacuum chamber is to intercept less than 10% of the radiation generated so as to avoid an impractical power loading on the crotch and side walls, the vacuum enclosure needs to be quite wide. With respect to pumping requirements there is a weak trade-off between increasing the static load from widening the chamber and minimizing the dynamic load by avoiding the photon fan. In the wigglers, which occupy only 2% of the circumference of the ring, we have relaxed the required operating pressure to 10 nTorr at the maximum design current.

Although focusing in the wiggle (horizontal) plane could be accomplished with canted or curved pole faces or with quadrupoles built into the wiggler, we have opted for a quadrupole triplet located between segments, L_2 and L_3 in order to maintain flexibility in tuning the lattice over a range of beam energies. This consideration

suggests the use of the tapered chamber illustrated in Fig. 1. To maintain a practical quadrupole design, the width, W_1, should be as narrow as practical. Balancing the difficulty of fabricating a large, split quadrupole with that of handling a large power density on the walls becomes another, stronger design trade-off. An example of the variation of synchrotron radiation power deposited along the vacuum chamber is given in Fig. 5.

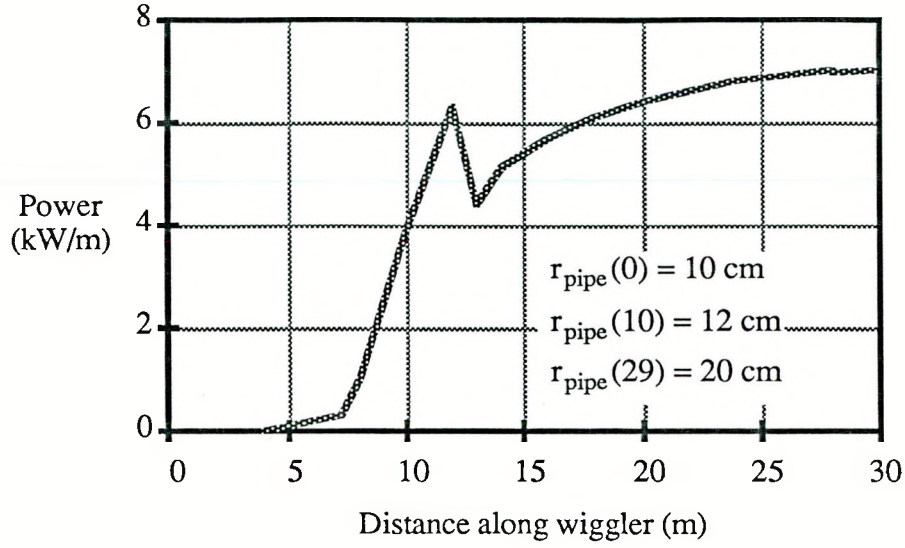

Figure 5. The thermal loads on each of the side walls of the wiggler vacuum chamber

From the linear power density we compute the dynamic gas load due to photo-desorption as follows. In a traversing a period of the wiggler, λ_w (cm) in dipole field of magnitude B the beam will emit a number of photons per second of synchrotron radiation given by

$$\dot{N}_\gamma = 3.85 \times 10^{17} \; I(A)\, B(T)\, \lambda_w(cm) \;, \tag{33}$$

where B is the average field of the wiggler; i.e.,

$$\begin{aligned} B &= B_{dipole}\; F_{fill} \quad \text{(bend-drift)}\,, \\ &= \frac{2}{\pi}\, B_w \quad \text{(standard wiggler)}. \end{aligned} \tag{34}$$

The synchrotron radiation power generated per period is $U_{o,w}\, I$. Hence, the number of gammas produced per MW is

$$\frac{d\dot{N}_\gamma}{dP} = 3.85 \times 10^{17}\; \frac{B(T)\, \lambda_w\,(cm)}{U_{o,w}\,(MeV)} \text{ photons/MW}\,, \tag{35}$$

where $U_{o,w}$ is given by Eq. (4) or (5) as appropriate to the configuration. For the bend-drift configuration

$$\frac{d\dot{N}_\gamma}{dP} = \frac{3.04 \times 10^{19}}{E^2 B_w} \text{ photons/kW}, \tag{36a}$$

while for the standard wiggler

$$\frac{d\dot{N}_\gamma}{dP} = \frac{3.88 \times 10^{19}}{E^2 B_w} \text{ photons/kW}. \tag{36b}$$

The desorbed gas load is related to the deposited power density by

$$Q \text{ (Torr-l/s/m)} = 3 \times 10^{-20} \left(\frac{d\dot{N}_\gamma}{dP} \right) \times \left(\frac{dP}{dL} \right) \eta_\gamma, \tag{37}$$

where η_γ is the local photo-desorption coefficient.

In the configuration calculated the chamber half-width, r_{pipe}, is initially 10 cm tapering gently to 12 cm at the end of L_2, whereupon the chamber tapers outward at ≈ 4 mrad to a half-width of 20 cm at the end of segment L_4. The dip in the linear power density at 12 m is due to the introduction of the taper. With this power density profile the maximum distributed pumping required is ≈210 l/s/m at L_4.

From Eq. (6) we can estimate that at 3 A, the power density in the forward direction will be 2.2×10^5 W/mr^2. From Eq. (10) and (11), we find that ≈80% of the radiation is emitted into 8.1 mrad^2. The photon dump must be placed at a distance from the end of the wiggler at which the power density is limited to the maximum acceptable value of 1 kW/cm^2. The distance to the dump, L_D, can be foreshortened by tilting the dump at an angle of 340 mrad with respect to the horizontal. For a tilted dump L_D should be 44 m. Although ≈20% of the radiation power will actually be deposited on the side walls of the chamber surrounding the wiggler, we compute the gas load at the photon dump assuming that all of the radiation is incident on the dump. If the dump is made of well cooled, oxygen free copper, the photo-desorption coefficient should rapidly fall to 2×10^{-6} molecules per photon. The gas load from such a dump will be $Q_{dump} = 1.6 \times 10^{-4}$ Torr-l/s.

By considering the flared vacuum chamber from the wiggler to the dump to be a long, differentially pumped manifold, we can allow the pressure at the dump to rise to a much higher value than in the beam pipe. At the dump the maximum horizontal extent of the radiation fan is 2.15 m while the vertical extent of the radiation is only 2 cm. To lower the conductance of the photon channel, we take the chamber height to be 8 cm with baffles of 1.8 cm aperture from the exit of the wiggler out to a distance of 22 m ($L_D/2$) and baffles of 3.5 cm aperture thereafter. This configuration yields a conductance of 260 Torr-l/s. The minimum total pumping of the dump plus photon channel is obtained by choosing the pressure to be 60 nTorr. This pressure

requires 2700 l/s of pumping at or near the dump that could be provided with large cryo-pumps. At $L_D/2$ 700 l/s of pumping will reduce the pressure to 45 nTorr. Distributed pumping of 55 l/s along the first half of the photon channel reduces the pressure to 10 nTorr at the exit of the wiggler.

A C-frame dipole magnet 5 m down stream from the exit of the wiggler exit bends the electron beam out of the radiation fan and into the straight beamline. The crotch can thereby be located away from the radiation fan of the wiggler. The straight beam pipe leaving the crotch should be a special narrow section of stainless steel with an inner radius of ≤3 cm. In this section lumped ion pumps providing 100 l/s from a point 10 m beyond the crotch extending downstream 5 m will reduce the pressure to 3 nTorr. At this point a transition section will match the beam pipe to the standard straight sections of vacuum chamber.

The broad radiation fan produced by the bend-drift wiggler configuration leads to a formidable radiation management scheme. An alternative design of the wiggler, which we have not matched into the low energy ring lattice, uses a standard sinusoidally varying field. In that case we have considered the effect of reducing the dimensionless vector potential of the wiggler by lowering the wiggler period as much as possible consistent with keeping B_w at or below the maximum permissible field. In that case we would need 2 wigglers with characteristics,

$$B_w = 1.8\ \text{T}, \quad \lambda_w = 32\ \text{cm.}, \quad L_w = 24\ \text{m.}$$

For this design, K is reduced to 53.1, which has the advantage of projecting the radiation into a narrow cone of half-angle 8.8 mrad in the horizontal plane. The vertical extent is unaffected. The vacuum chamber in the vicinity of the wiggler (Fig. 6) can have a constant width of 32 cm with ≈140 l/s/m of pumping needed in the final 20% of the wiggler to assure an operating pressure of 10 nTorr. The maximum thermal load on each wall in this region at the end of the wiggler is 3.9 kW/m.

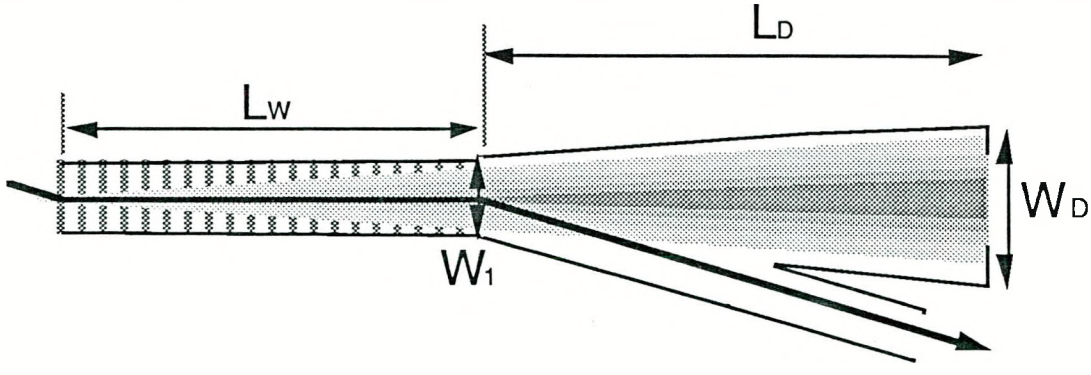

Figure 6. The geometry of the standard wiggler configuration.

A superior design of the vacuum chamber is to taper the chamber gently from a width of 20 cm at the beginning of the wiggler to a width of 16 cm at the end. The 2.5 mrad taper spreads the flux sufficiently that the pumping needed is reduced

to 95 l/s/m at the end of the wiggler and the peak thermal load on each side wall is only 2.6 KW/m. The two chamber designs are compared in Fig. 7. In both cases the thermal load is restricted to the final 20% of the vacuum chamber surrounding the wiggler.

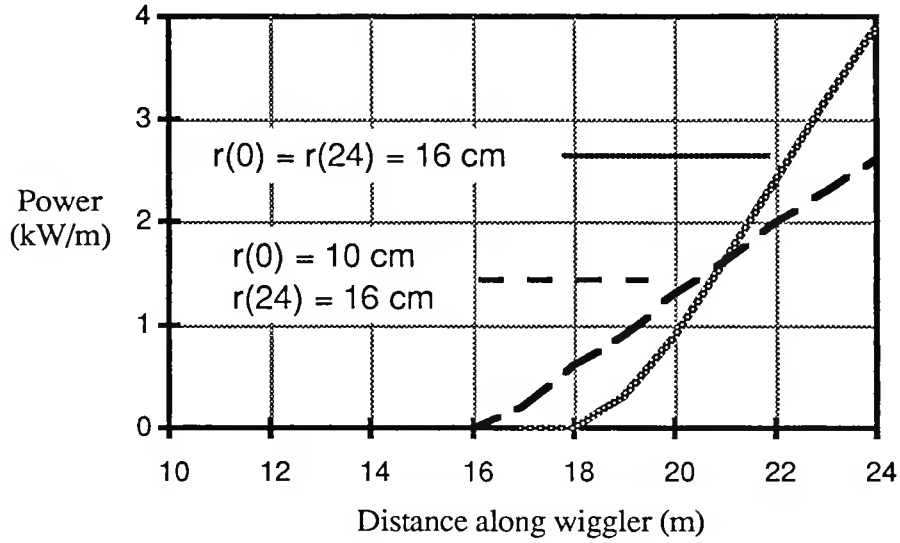

Figure 7. Variation in power density on each side wall with standard wiggler

To compare the dump requirements for this design with those for the bend-drift wiggler, we change the inclination of the surface of the dump to 250 mrad and leave the maximum power density and the distance from the end of the wiggler to the dump the same, i.e., 44 m. In this case the width of the radiation fan at the dump is reduced to 1.2 m. hence, the conductance of the flared photon channel is reduced to 160 Torr-l/s. As the average bending field is different in the two wiggler configuration, the number of photons per kW of radiation power will also be different as specified in Eq. (36). Consequently, the gas load at the dump for the standard wiggler is somewhat larger than that for the bend-drift design, i.e., $Q_D = 1.9 \times 10^{-4}$ Torr-l/s.

The total pumping of the photon channel is now minimized by operating the dump at a pressure of 235 nTorr, which requires 1240 l/s of pumping at the dump. At $L_D/2$ 830 l/s of lumped pumping will reduce the pressure to 80 nTorr. From this point to the end of the wiggler, pumping of 50 l/s/m will differentially pump the photon channel to 10 nTorr at the exit of the wiggler. Vis á vis the bend-drift configuration the total pumping of the standard wiggler configuration is reduced by >900 l/s in the photon channel and by ≈4000 l/s in the wiggler channel. The impact of the choice of configuration on the overall cost and performance of the collider requires further detailed study.

CONCLUSIONS

Damping wigglers in the low energy ring of the B factory can provide energy transparency albeit at the price of a formidable design task. The magnets which constitute the wiggler will require a large horizontal aperture if radiation loads on the side walls of the vacuum chamber are to be kept to manageable levels. Appropriate tapering of the chamber can lead to an appreciable reduction in the thermal loads and *a fortiori* the dynamic gas loads. The most challenging problem is that of dumping the photon beam in a way that assures the integrity of the dump under all operating conditions and which can accommodate the enormous dynamic gas loads generated by multi-MW beam X-ray beams. Stainless steel vacuum chambers can provide adequate shielding of wiggler magnets from the synchrotron radiation. Stainless steel also has sufficient strength to assure the mechanical stability of the photon channel.

Some of the difficulties of designing the photon dump and vacuum system can be ameliorated by adopting a wiggler of standard configuration; i.e., one with a field varying sinusoidally along the beam path. Another means of reducing the gas load generated at the photon dump may be to use a set of metal layers chosen to reduce the opacity of the dump at the critical energy of the photon beam. In that way the photons, which are normally incident on the dump penetrate deeply, reducing the photo-desorption probability. Still given the size of the damping wiggler with its accompanying vacuum chamber and pumping system, the price of providing energy transparency will not be low. A more aggressive design of the bending magnets and vacuum system in the low energy ring arcs can lessen but not eliminate the design difficulties that attend wigglers producing megawatt X-ray beams. Hence, an important topic for research is determining how much energy transparency is worth the price.

ACKNOWLEDGEMENTS

I wish to thank Alper Garren, Kwang-je Kim and Michael Zisman of LBL and Alexander Varfolomeev of the Kurchatov Institute, Moscow, for several helpful discussions concerning wiggler options for the B factory. Work partially performed under the auspices of the U.S.Department of Energy by the Lawrence Livermore National Laboratory under contract No. W-7405-Eng-48.

Technical Information Department · Lawrence Livermore National Laboratory
University of California · Livermore, California 94551